J. Synchrotron Rad. (1998). **5**, 569–571

Performance of the VUV beamline 4.1 at the SRS, Daresbury Laboratory

V. R. Dhanak,[a]* A. G. Shard,[a] C. A. Muryn,[b] P. L. Wincott[b] and G. Thornton[b]

[a]Surface Science Research Centre, University of Liverpool, PO Box 147, Liverpool L69 3BX, UK, and [b]Interdisciplinary Research Centre in Surface Science and Chemistry Department, Manchester University, Manchester M13 9PL, UK. E-mail: vin@ssci.liv.ac.uk

(*Received 5 August 1997; accepted 22 September 1997*)

The performance of a recently commissioned beamline, designated BL4.1, at the SRS, Daresbury Laboratory, is described. This beamline covers the energy range $15 \geq h\upsilon \geq 200$ eV, using a spherical grating monochromator, and is equipped with a UHV surface-science endstation containing a Scienta SES200 and an HA54 angle-resolving electron-energy analyser. Design parameters and optical specifications are tabulated. Monochromator resolution has been determined by measuring the Fermi edge of a Pt foil cooled to 40 K and these values are compared with the calculated resolution. The flux delivered to the endstation has been measured directly using a calibrated photodiode. The performance of the beamline is further illustrated by reference to a study of the angular distribution of photoemitted intensity from a band-gap state on a $TiO_2(110)$ 1×2 surface.

Keywords: spherical grating monochromators; surface science; VUV.

1. Introduction

In a previous paper (Dhanak *et al.*, 1992), we described the conceptual design and characteristics of the grazing incidence spherical grating monochromator (SGM) beamline on bending magnet 4 at the Synchrotron Radiation Source (SRS), Daresbury Laboratory. Its main purpose is to provide a facility for the Interdisciplinary Research Centre in Surface Science with which to carry out angle-resolved and angle-integrated photoemission measurements, photoelectron diffraction and dichroism studies. The beamline, which is designated BL4.1, is optimized for operation in the energy range $15 \geq h\upsilon \geq 200$ eV, which allows electronic structure to be probed through excitation of shallow core levels and the valance band. The design concept and the advantages of this type of monochromator have been discussed in detail elsewhere (Chen, 1987). In this article we briefly describe the geometrical layout, operation and performance of the beamline, which has recently been constructed and commissioned.

2. Beamline layout and parameters

The concept and design of the beamline is based on the Dragon beamline at NSLS, Brookhaven National Laboratory (Chen, 1987; Chen & Sette, 1989). Its main design strategy is to use simple and separate optical elements to decouple the focusing in the horizontal and vertical directions. A schematic layout of the beamline is shown in Fig. 1. The geometrical parameters and optical specifications are detailed in Table 1. At the left in Fig. 1 are two pre-mirrors close to each other. The focusing function of the two mirrors is decoupled. The one closest to the source is the horizontally focusing mirror (HFM) and the second is the vertically focusing mirror (VFM). The HFM is water cooled since it serves as a heat and radiation sink, protecting the other optical elements in the line. It collects 6 mrad of the available synchrotron radiation at dipole 4, deflects the beam sideways and focuses the source horizontally in the non-dispersive direction at the mean position of the monochromator exit slit. The VFM deflects the beam upwards and focuses vertically in the dispersive

Table 1
Beamline parameters.

Source			
SRS Dipole 4			
Size (mm)		2×0.4	
Divergence (mrad)		6×2	
HFM			
Distance from source (m)		9.67	
Horizontal beam deflection (°)		13	
Cylindrical radius (m)		102.53	
Material		Pt on Glidcop, water-cooled	
Active optical area (mm)		570×42	
Slope error (arcsec)		10	
Microroughness (nm)		1.0 r.m.s.	
VFM			
Distance from HFM (m)		3	
Vertical beam deflection (°)		8	
Cylindrical radius (m)		90.63	
Material		Pt on Glidcop	
Active optical area (mm)		400×70	
Slope error (arcsec)		0.5	
Microroughness (nm)		0.5 r.m.s.	
Demagnification		3	
Entrance slit			
Distance from VFM (m)		4.212	
Traverse (mm)		±50	
Slit width (mm)		0.005–3.00	
Slit length (mm)		35	
Spherical grating monochromator			
Distance from entrance slit, r (m)		2.818	
Included angle (°)		164	
Spherical radius (m)		26.19	
Grating material		Au on fused silica	
Active optical area (mm)		35×150	
Diffraction order		Positive 1	
Maximum rotation from zero order (°)		4	
Rotation step accuracy (arcsec)		0.5	
Gratings energy range (eV)	15–45	45–130	130–220
Groove density (mm^{-1})	204	597	1500
Laminar groove depth (nm)	600	235	160
Laminar groove width (nm)	2549	1005	480
Microroughness (nm)		0.5 r.m.s.	
Slope error (arcsec)		<1	
Translatable exit slit			
Distance from grating, r' (m)		4.484	
Traverse (mm)		300	
Slit width (mm)		0.005–3.00	
Slit length (mm)		35	
Refocusing ellipsoidal mirror			
Distance from exit slit (m)		2.546	
Beam deflection (°)		8	
Semi-major axis (m)		1.773	
Semi-minor axis (m)		0.1113	
Active optical area (mm)		300×40	
Material		Pt on Glidcop	
Distance from sample (m)		1.0	
Slope error (arcsec)		2	
Microroughness (nm)		0.5 r.m.s.	

direction at the monochromator entrance slit. An aperture (MXD) upstream of the VFM is located to allow selection of circular polarized light in the upper or lower part of the photon beam in the vertical direction for dichroism experiments.

After the entrance slit, one of three *in situ* interchangeable gratings diffracts and focuses the photon beam vertically at the exit slit. The Au-coated spherical gratings are holographically recorded ion-etched laminar profiles on quartz blanks and were manufactured by Carl Zeiss Ltd. The exit slit is made movable in order to follow focusing at different energies. Tolerence for this movement is not critical and the maximum movement from the mean position is about 300 mm for each of the gratings. The slits are continuously variable parallelograms. The slit mechanism, monochromator, coupling and scanning mechanism, as well as the mirror vessels, were engineered and manufactured by Bird and Tole Ltd.

After the exit slit, there is a post-focusing ellipsoidal mirror which focuses the photon beam to a spot measuring about 2 × 0.5 mm. The pre- and post-mirrors are Pt coated on Glidcop and manufactured by Photon Sciences International.

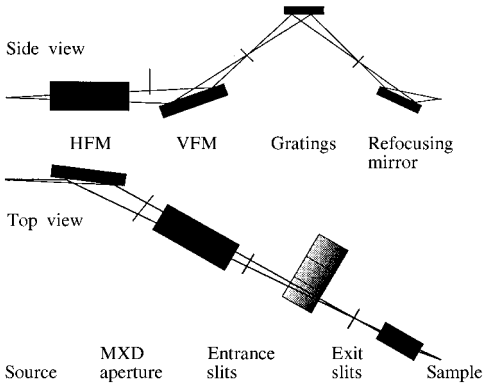

Figure 1
Schematic layout of beamline 4.1 at the SRS.

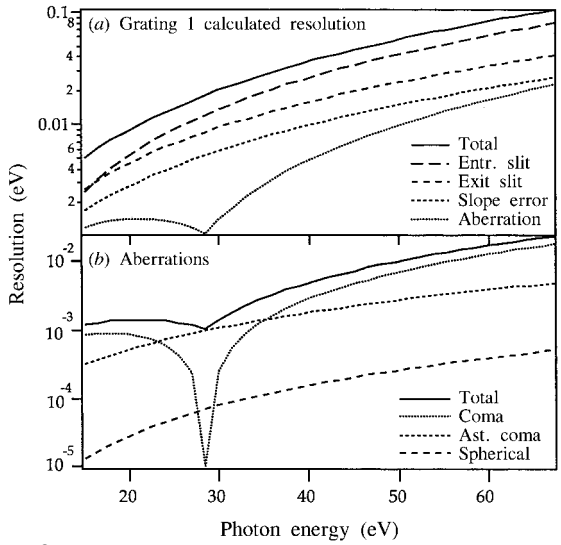

Figure 2
Calculated photon-energy resolution. The entrance and exit slits were set to 100 μm. The aberration term was calculated using absolute values for the coma term.

3. Resolution and flux

Photon-energy resolution in a spherical grating monochromator is defined by the entrance slit, which represents the source size, as well as the exit slit, grating aberrations and slope errors. Calculated contributions to the resolution due to each of these elements together with the sum of these contributions for beamline 4.1 are shown in Fig. 2(*a*) for the first grating. The entrance and exit slits were set to 100 μm in the calculations. This value for the entrance slit corresponds to just below the ideal source size for our beamline. The illuminated grating surface area was set to 30 mm (dispersive direction) × 17.5 mm. Grating aberrations include the primary coma, astigmatic coma and spherical contributions. The defocus term is eliminated by moving the exit slit. These contributions to the total aberration are shown in Fig. 2(*b*), where we have plotted the absolute values. The values were calculated from analytical expressions (Chen & Sette, 1989) using the parameters given in Table 1. Under these conditions, it is seen in Fig. 2 that the resolution is dominated by the source size defined by the entrance slit. Similar results have been obtained for the second and third gratings. The calculated total resolution for each of the gratings is shown in Fig. 3.

To determine the resolution of the beamline experimentally, we have measured the Fermi level of a Pt foil mounted on a

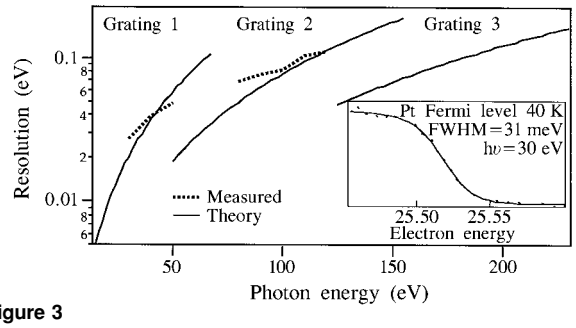

Figure 3
Measured resolution compared with the total calculated values. The inset shows the Fermi level from a Pt foil measured at a photon energy of 30 eV. The fit is also shown, as a solid line, yielding a Fermi function width of 31 ± 2.2 meV.

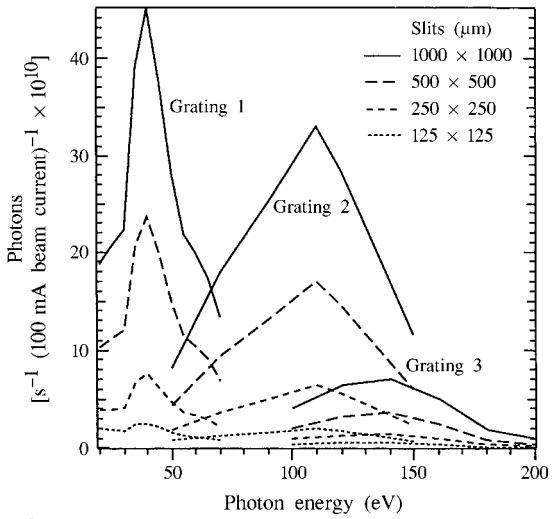

Figure 4
Absolute photon flux as a function of photon energy, measured for different slit settings.

liquid-helium-cooled sample stage. The sample temperature was approximately 40 K, at which temperature the Fermi function natural width is less than 15 meV. Photoemission at the Fermi level was measured using a Scienta 200 hemispherical electron-energy analyser with a pass energy and analyser slit set to give an inherent electron-energy resolution of about 12 meV (FWHM). The combined linewidth due to the analyser and the Pt Fermi level was therefore less than 18 meV. This was checked using an HeI line ($h\upsilon = 21.2$ eV) from a laboratory source and the width of the Fermi function was measured to be 18 meV. Measurements were then made using different photon energies from the first two gratings with the entrance and exit slits set at 100 × 100 μm. The Pt 5*d* cross section is unfavourable for measurements from the third grating. The results are shown in Fig. 3, which also shows in inset an example of the Pt Fermi edge measured at a photon energy of 30 eV with a combined Fermi function width of about 30 meV, indicating a photon-energy resolution of 25 meV, *i.e.* a resolving power of 1200. The count rate in the Scienta analyser was about 300 counts s^{-1} under these conditions, which is acceptable. The measured curves show that the photon-energy resolution is in close agreement with the calculated total resolution.

From Fig. 2 it is clear that by closing the entrance and exit slits further one can achieve the theoretical resolution limit set by the grating aberrations and the slope error. However, in reality, for many surface-science experiments, resolution is not the only factor. Often the cross section of core levels is weak or the sample system of interest is dilute. In such cases the flux delivered by the beamline becomes important and the slits have to be opened at the expense of resolution. We have measured the flux as a function of photon energy at the sample for different slit openings using a calibrated photodiode from International Radiation Detectors Inc. The results are displayed in Fig. 4 and show that the photon flux varies in an expected way for different slit sizes and agrees reasonably well with calculated flux from the beamline presented by Dhanak *et al.* (1992). The measured photon flux is comparable to that from similar dipole beamlines at the SRS and other second-generation sources. The resolving power for a slit size of 500 × 500 μm is estimated to be better than 500 while for the 125 × 125 μm slit setting we are able to achieve 1000. These values represent the extremes for setting up the beamline for most surface-science users on this beamline.

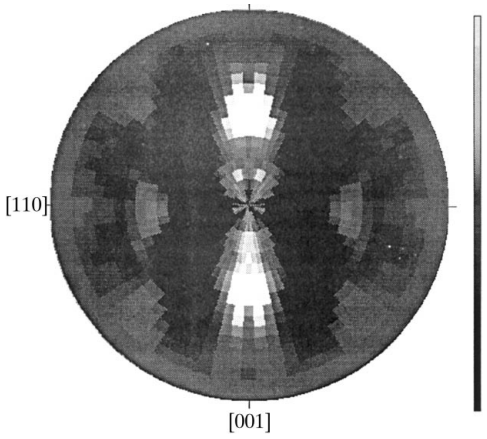

Figure 5
Resonant photoemission angular distribution map of the Ti 3*d* band-gap state on TiO_2(110) 1 × 2. BE = 0.8 eV, $h\upsilon = 47$ eV.

4. Photoelectron angular distributions

The beamline has been in routine operation for about two years and a number of successful experiments have been performed, from band-mapping studies to measuring core levels, from metal to oxide surfaces. Recently, we have also measured linear and circular dichroism from Fe films on W(110) using the Fe 3*p* core photoemission. In order to illustrate the performance of the beamline in terms of photoemission intensity, we present in Fig. 5 a 2π intensity map of the band-gap state on TiO_2(110) 1 × 2 at the resonant photon energy of 47 eV. This was recorded by stepping the sample manipulator with the Scienta SES200 analyser fixed. The map was recorded by setting an azimuthal scan of 270°, synchronized about 110°, in 2° steps for each 2° shift in polar angle from normal to grazing-electron emission angle (full range, normal to 80° off normal). The image, which is presented symmetrized along the [110] azimuth, shows the intensity of *d*-orbital lobes oriented along the [001] azimuth from atomic like defects on the TiO_2(110) 1 × 2 surface, consistent with an added row model for this surface.

5. Conclusions

The performance of the VUV beamline 4.1 at the SRS, Daresbury Laboratory, has been described in terms of the measured resolution and flux compared with calculated values. The resolving power has been demonstrated to be better than 1000 with the limiting factor being the source size defined by the entrance slit. The beamline station is equipped with a Scienta SES200 analyser which, combined with the performance of the photon beam, allows a variety of experiments to be performed. An illustrative study measuring photoemission angular distribution is presented.

This work was funded by the EPSRC (UK). The authors thank H. Padmore, C. S. Mythen and G. van der Laan for their contributions during the design and calculation stages of the beamline, and are grateful to P. Hardman for making the photoelectron diffraction measurements.

References

Chen C. T. (1987). *Nucl. Instrum. Methods*, **256**, 595–604.
Chen, C. T. & Sette, F. (1989). *Rev. Sci. Instrum.* **60**, 1616–1621.
Dhanak, V. R., Robinson, A. W., van der Laan, G. & Thornton, G. (1992). *Rev. Sci. Instrum.* **63**, 1342–1345.